Effect of Ni doping on vortex pinning in $CaK(Fe_{1-x}Ni_x)_4As_4$ single crystals

N. Haberkorn,[1,2] M. Xu,[1,3] W. R. Meier,[1,3] J. Schmidt,[1,4] S. L. Bud'ko,[1,3] and P. C. Canfield[1,3]
[1]*Ames Laboratory, U.S. Department of Energy, Iowa State University, Ames, Iowa 50011, USA*
[2]*Centro Atómico Bariloche and Instituto Balseiro, CNEA and Consejo de Investigaciones Científicas y Técnicas Av. E. Bustillo 9500, R8402AGP, S. C. Bariloche, RN, Argentina*
[3]*Department of Physics and Astronomy, Iowa State University, Ames, Iowa 50011, USA*
[4]*Departamento de Física, FCEyN, and IFIBA-CONICET, Universidad de Buenos Aires, Buenos Aires 1428, Argentina*

(Received 3 July 2019; published 28 August 2019)

We study the correlation between chemical composition and vortex dynamics in Ni-doped $CaK(Fe_{1-x}Ni_x)_4As_4$ ($x = 0$, 0.015, 0.025, 0.03, and 0.05) single crystals by performing measurements of the critical current densities J_c and the flux creep rates S. The magnetic relaxation of all the crystals is well described by the collective creep theory. The samples display a glassy exponent μ within the predictions for vortex bundles in a weak pinning scenario and relatively small characteristic pinning energy ($U_0 < 100$ K). The undoped crystals display modest J_c values at low temperatures and high magnetic fields applied along the c axis. $J_c(T)$ dependences at high fields display an unusual peak. The enhancement in $J_c(T)$ matches with an increase in U_0 and the appearance of a second peak in the magnetization. As Ni doping increases, whereas there is a monotonic decrease in T_c there is a nonmonotonic change in J_c. Initially J_c increases, reaching a maximum value for $x = 0.015$, and then J_c decreases for $x \geqslant 0.025$. This change in $J_c(x)$ is coincident with the onset of antiferromagnetic order. The magnetic field dependence of $J_c(H)$ also manifests a change in behavior between these x values. The analysis of the vortex dynamics for small and intermediate magnetic fields shows a gradual evolution in the glassy exponent μ with Ni content, x. This implies that there is no appreciable change in the mechanism that determines the vortex relaxation.

DOI: 10.1103/PhysRevB.100.064524

I. INTRODUCTION

The critical current densities J_c in type-II superconductors depend on a complex interplay of individual pinning centers, the interaction between vortices, and thermal fluctuations [1,2]. The discovery of iron-based superconductors (Fe-SCs) has allowed for an expansion of the knowledge about the influence of intrinsic superconductor parameters on the resulting vortex dynamics [3,4]. The different families of Fe-SCs display superconducting transition temperatures T_c up to 56 K [5–7]. These materials usually exhibit strong interplay between superconductivity and magnetism [8]. The electronic properties depend on doping (substitutional disorder) and are also affected by pressure [5–7,9–11]. Vortex dynamics in Fe-SCs is usually well described by the collective creep theory [12–14]. The sources of flux pinning include random point defects [15], precipitates [16], planar defects [17], and correlated disorder such as twin boundaries [18]. Notwithstanding the coexistence between superconductivity and magnetism usually present in many Fe-SCs [19–21], its influence on the resulting vortex dynamics has been little explored.

Current-carrying capacity is a relevant parameter which determines the range of applications of new superconducting materials. Single crystals are the starting point to evaluate vortex pinning mechanisms. Temperature T and magnetic field H dependences of J_c in any superconductor depend on the type and density of pinning centers. The $J_c(H)$ dependences in Fe-SCs usually display several regimes as a consequence of a pinning landscape with random point disorder and a low density of large defects [15]. Depending on the disorder at the nanoscale, the $J_c(H)$ curves may decrease monotonically or display a second peak in the magnetization (SPM) or fishtail [12–14]. On the other hand, because of thermally activated vortex motion, J_c data usually decrease with temperature. An exception to that has been recently observed in $CaKFe_4As_4$ single crystals [16,17,22,23]. For instance, as a consequence of smoother $J_c(H)$ dependences, the J_c value for $\mu_0 H = 5$ T at 20 K is higher than that observed at 10 K. This unusual behavior has been related to the presence of planar $CaFe_2As_2$ intergrowths [16].

$CaKFe_4As_4$ is a member of the so-called 1144 family $AeAFe_4As_4$ ($Ae =$ Ca, Sr, Eu, and $A =$ K, Rb, Cs). $CaKFe_4As_4$ has a tetragonal structure ($P4/mmm$), where Ca and K layers stack alternatively across the Fe_2As_2 layer along the c axis [24]. The undoped compound is a multiband superconductor with $T_c \approx 35$ K with no other identified phase transition (magnetic or structural) [24–26]. Under pressure, T_c is suppressed and then superconductivity disappears at $p \geqslant 4$ GPa due to a structural phase transition into a half-collapsed tetragonal state [27]. The extrapolated upper critical field at zero temperature for $CaKFe_4As_4$ is $\approx$70 T with a coherence length $\xi_{GL}(0) \approx 1.4$ nm [25]. The anisotropy parameter $\gamma = H_{c2}^{\perp c}/H_{c2}^{//c}$ for $\mathbf{H}$ applied perpendicular and parallel to the c axis increases, with the temperature being 1.5 at 25 K and 2.5 near T_c [26]. The penetration depth estimated using muon-spin rotation is $\lambda(0) = 208\,(4)$ nm [28]. Although no substitutional disorder is expected, low-temperature scanning tunneling microscope (LT-STM) data reveal the presence of locations with suppression of the superconducting order

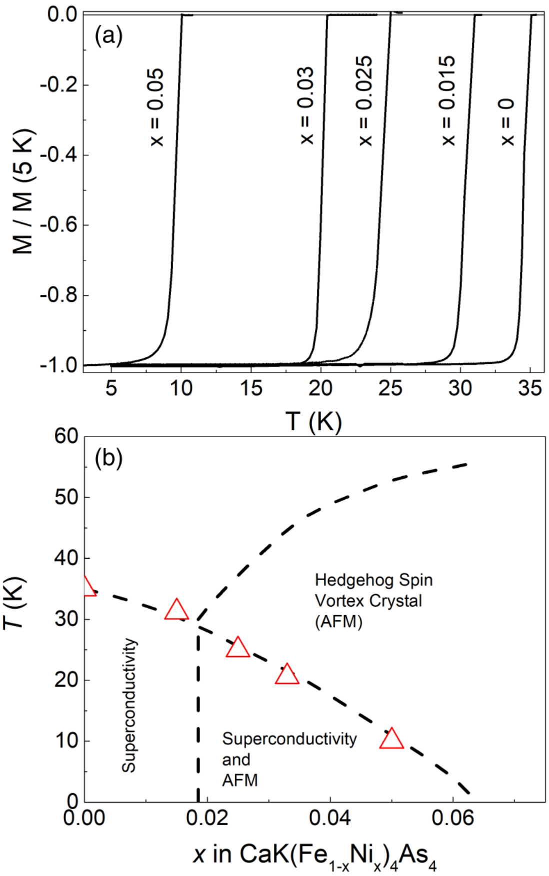

FIG. 1. (a) Temperature dependence of the normalized magnetization [M (T) /M (5 K)] for the studied single crystals. The measurements were performed with $\mu_0 H = 0.5$ mT and **H** // c. (b) Corresponding Ni doping for the studied crystals on a schematic magnetic phase diagram of $CaK(Fe_{1-x}Ni_x)_4As_4$ single crystals [21,30].

parameter [29]. Gradual suppression of the T_c and the emergence of magnetic order take place via Co or Ni substitution onto the Fe site [30,31]. As shown in Fig. 1(b), coexistence of superconductivity and antiferromagnetism (AFM) appears for adequate doping [21]. Moreover, the Ni/Co addition should modify the vortex pinning landscape by introducing disorder due to chemical substitution.

In this work, we analyze the influence of the Ni doping on the vortex dynamics of $CaK(Fe_{1-x}Ni_x)_4As_4$ single crystals ($x = 0$, 0.015, 0.025, 0.03, and 0.05) by performing magnetization measurements. We systematically study the influence of the Ni addition on the J_c (T, H) dependences. The vortex dynamics are analyzed in the framework of the collective creep theory [32]. We measure the flux creep rate $S = -^{\delta \ln J_c}/_{\delta \ln t}$ as a function of the temperature and the magnetic field. The effective barrier height for flux creep rates and glassy exponent μ are analyzed by the extended Maley method [33].

II. EXPERIMENTAL

Single crystals of Ni-doped $CaKFe_4As_4$ were grown out of a high-temperature solution rich in transition metals and arsenic, similar to the procedure used for the pure compound [26,30,34]. The study is performed using $CaK(Fe_{1-x}Ni_x)_4As_4$ single crystals with $T_c = 35$ K ($x = 0$), 31.1 K ($x = 0.015$), 25 K ($x = 0.025$), 20.5 K ($x = 0.03$), and 10.1 K ($x = 0.05$). The single crystals exhibit a platelike morphology with the c axis perpendicular to the plane of the plate. The samples used were roughly rectangular plates with length l, width w, and thickness d. The magnetization (M) measurements were performed using a superconducting quantum interference device (SQUID) magnetometer. The thicknesses d were calculated using the area ($l \times w$) and the superconductor volume and Meissner slopes with $\mathbf{H}//ab$ considering the proper demagnetization factor. The volume and the mass of all the studied single crystals agree with the density determined from lattice parameters, 5.22 g/cm^3 [24]. The J_c values were calculated from the magnetization data using the appropriate geometrical factor in the Bean model [35,36]. For $\mathbf{H}\|c$, $J_c = \frac{20\Delta M}{w[1-w/(3l)]}$, where ΔM is the difference in magnetization M (emu/cm^3) between the top and bottom branches of the hysteresis loop. The creep measurements $M(t)$ were recorded over a time greater than 60 min. The magnetization of the sample holder was measured and subtracted from the data by averaging the initial points of the time relaxation for the lower and upper magnetic branches. The initial time was adjusted considering the best correlation factor in the slope of $S = -^{\delta \ln J_c}/_{\delta \ln t}$. The initial critical state for each creep measurement was generated using $\Delta H \sim 4H^p$, where H^p is the field for full flux penetration, estimated as $H^p = {}^{J_c d}/_2$ [37].

TABLE I. Summary of superconducting properties in the $CaK(Fe_{1-x}Ni_x)_4As_4$ single crystals. (α) corresponds to the exponent of the power-law regime obtained from $J_c(H)$ at 5 K.

Sample	T_c (K)	J_c^{sf}(5 K) (MA cm^{-2})	α	Thickness (μm)
$CaKFe_4As_4$	35.0	1.7	0.68	34
$CaKFe_4As_4$	35.0	2.0	0.68	14
$CaK(Fe_{0.985}Ni_{0.015})_4As_4$	31.1	2.8	0.56	25
$CaK(Fe_{0.975}Ni_{0.025})_4As_4$	25.0	1.7	0.47	37
$CaK(Fe_{0.97}Ni_{0.03})_4As_4$	20.5	1.3	0.46	58
$CaK(Fe_{0.95}Ni_{0.05})_4As_4$	10.1	0.1	0.40	38

III. RESULTS AND DISCUSSION

Figure 1(a) shows the temperature dependence of the normalized magnetization [M (T) /M (5 K)] for the studied single crystals. The measurements were performed with **H** // c axis under zero-field cooling (ZFC) with an applied magnetic field of 0.5 mT. The T_c value decreases systematically from 35 K for the undoped single crystal to ≈10.1 K for $CaK(Fe_{0.95}Ni_{0.05})_4As_4$ (see Table I). Figure 1(b) shows a schematic x-T phase diagram for $CaK(Fe_{1-x}Ni_x)_4As_4$ and the corresponding position of the studied samples [30]. The single crystals with $x > 0.02$ display coexistence of superconductivity and AFM order [21,30,31].

Figure 2 shows the $J_c(H)$ dependences at different temperatures for each chemical composition obtained from the hysteresis loops (see Appendix). The curves are plotted on log-log scales. Partial data at 1.8 K are shown due to flux jumps.

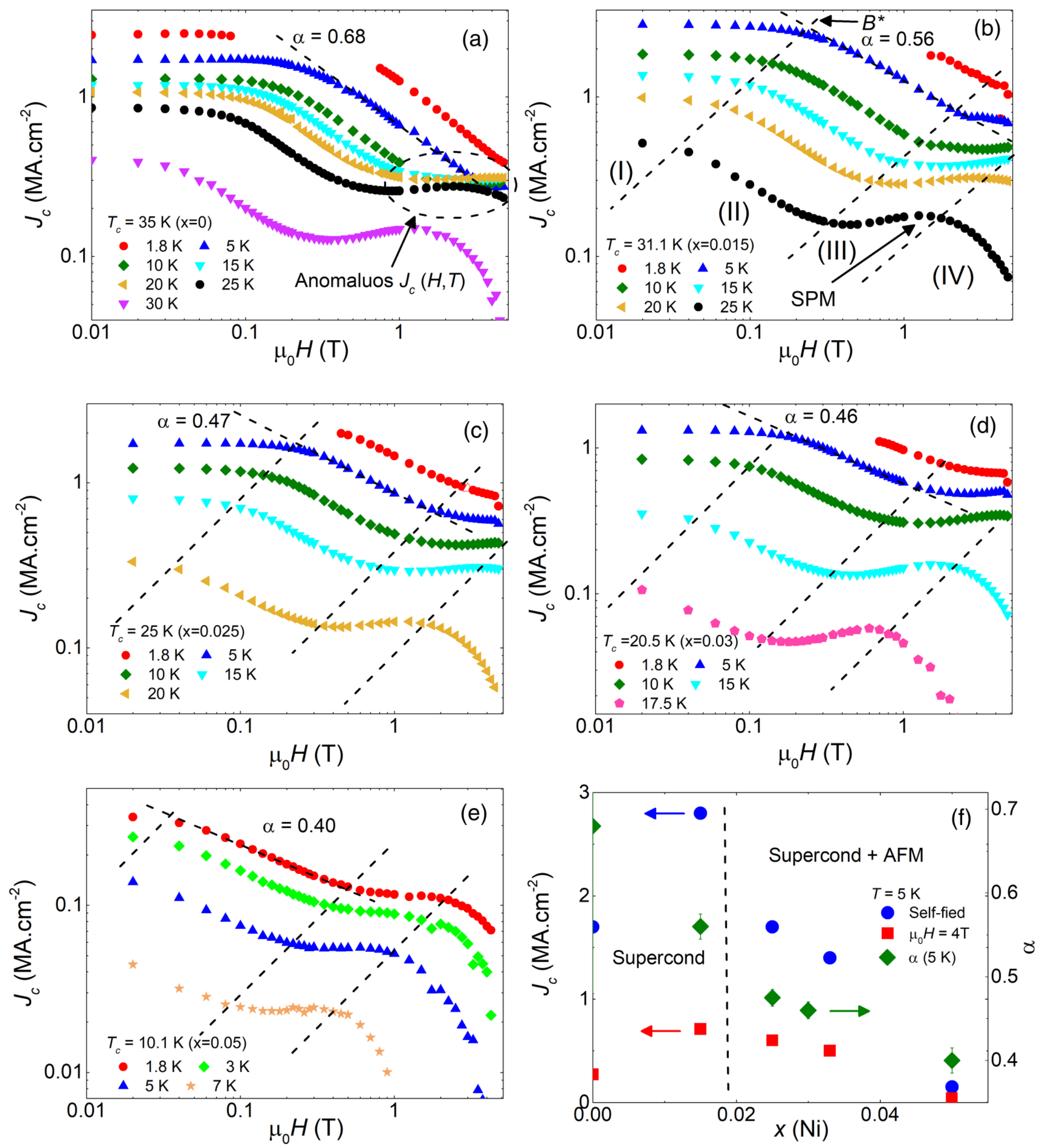

FIG. 2. (a)–(e) Magnetic field dependence of the critical current densities J_c at different temperatures for Ni-doped $CaK(Fe_{1-x}Ni_x)_4As_4$ single crystals. Partial curves at 1.8 K are shown due to the presence of flux jumps. (f) Ni doping dependence self-field critical current density J_c^{sf} and J_c (4 T) at 5 K (left axis) and α exponent (right axis). Dashed vertical line indicates the expected doping for coexistence between superconductivity and AFM [30]. The measurements were performed with **H** // c axis.

The $J_c(H)$ dependences display a low field saturation followed by a power-law regime, followed by a local maximum associated with a second peak in the magnetization (SPM). The latter becomes very weak at $x = 0.05$. The power law is related to a low density of strong pinning centers and the SPM to random point disorder [15]. The (J_c/J_0) ratio is a parameter that determines the strength of the pinning potential (with $J_0 = cH_c/3\sqrt{6}\pi\lambda \approx 170\,\mathrm{MA\,cm^{-2}}$, H_c the thermodynamic critical field, and c the speed of light) [32]. The undoped crystal displays a self-field of $J_c^{sf}(1.8\,\mathrm{K}) \approx 2.4\,\mathrm{MA\,cm^{-2}}$ and $(J_c/J_0) \approx 0.014$. The low fraction of J_0 is similar to that found in single crystals of other Fe-SCs [38,39]. Depending on the magnetic field strength, several regimes of the $J_c(H)$ behavior are observed [see Fig. 2(b)]: (I) a low-field regime ($B < B^*$) that could be associated with the single-vortex regime (SVR) but that is also strongly affected by the self-field; (II) a power-law dependence $J_c \propto H^{-\alpha}$ related to strong pinning centers; (III) a third regime (at the end of the power law) related to random disorder with $J_c(H) \approx$ constant or a SPM; and (iv) a high-field regime which is characterized by a fast drop in $J_c(H)$ and is usually related to a crossover from elastic to plastic relaxation of the vortex lattice [12]. As is usual, if the temperature increases, the in-field position at the maximum of the SPM decreases.

At first glance, there is a qualitative difference between the undoped and the doped samples related to regime III. The undoped crystals display an unusual maximum at $J_c(T)$ at intermediate temperatures [see Fig. 2(a)] [16,17,22,23]. The effect disappears for Ni-doped samples. In fact, the $J_c(H)$ curves are similar to those reported in other systems such as Co-doped $BaFe_2As_2$ [40,41] and $Ba_{1-x}K_xFe_2As_2$ [42,43]. However, unlike these Fe-SCs, the pinning in $CaK(Fe_{1-x}Ni_x)_4As_4$ cannot be related to orthorhombic structural domains [40,42]. Figure 2(f) (left axis) shows a summary of J_c^{sf} and J_c^{4T} at 5 K. Although the data correspond to different T/T_c values, it is useful to analyze the influence of the Ni addition on the J_c values at low and high magnetic fields. The results show that small Ni addition improves J_c in the whole range of magnetic fields, indicating that the disorder produced by chemical inhomogeneities enhances vortex pinning. The $J_c^{sf}(x)$ displays a maximum value of $2.8\,\mathrm{MA\,cm^{-2}}$ at $x = 0.015$ that systematically drops at larger doping. To rule out any effect related to the thickness (d) in the J_c^{sf} enhancement, we also measure a thinner undoped crystal (see Table I) [44]. Although J_c^{sf} increases from $1.7\,\mathrm{MA\,cm^{-2}}$ ($d = 34\,\mu$m) to $2.0\,\mathrm{MA\,cm^{-2}}$ ($d = 14\,\mu$m), its qualitative x dependence is unaffected.

It should be noted that both $J_c(x)$ and $\alpha(x)$ data [shown in Fig. 2(f)] show a clear change in behavior between $x = 0.015$ and 0.025, i.e., a clear change in behavior as the sample develops an AFM ordered ground state that coexists with a competing superconducting state. $J_c(x)$ for self-field shows a discontinuous break with a clear maximum on the low-x side ($x = 0.015$). $J_c(x)$ for $\mu_0 H = 4$ T also has a maximum value for $x = 0.015$. Whereas similar behavior was found for Co-doped $BaFe_2As_2$ [40], in the case of Ni-doped $CaKFe_4As_4$, structural domains associated with a low-temperature, orthorhombic structure are absent. If indeed the local maximum in J_c is associated with onset of hedgehog-spin vortex crystal AFM order [30,31], then this implies that AFM domains, not structural ones, are playing a key role. This change in pinning may also be responsible for the more gradual decrease in α in the antiferromagnetic state. The $J_c^{4T}(x)$ curve shows a broad maximum spanning from $x \approx 0.015$ to 0.03. The observed value of $J_c^{4T}(5\,K) \approx 0.27\,\mathrm{MA\,cm^{-2}}$ for the undoped crystal increases to $0.7–0.5\,\mathrm{MA\,cm^{-2}}$ for $x = 0.015–0.03$. The influence of the Ni addition on the pinning at high magnetic fields is also evident from the reduction of the J_c^{sf}/J_c^{4T} ratio. The analysis of the different vortex pinning regimes as a function of Ni doping is presented below.

Regimes (I) and (II) have been described by strong pinning produced by normal inclusions [15]. Regime (I) corresponds to the SVR and is limited by vortex-vortex interactions at B^* [see Fig. 2(b)]. However, experimentally the single-vortex pinning is overlapped by self-field effects ($B^* \approx J_c \times$ *thickness*), making its analysis difficult [45]. In addition to the changes in the absolute J_c values, the additional disorder at the nanoscale, produced by Ni substitution, modifies the power-law dependence $J_c \propto H^{-\alpha}$. The α values decrease systematically from $\approx$0.68 to $\approx$0.40 as the Ni doping increases [see right axis in Fig. 2(f) and Table I]. As we mentioned above, the α values go towards values smaller than 0.5, changing more gradually when AFM and superconductivity coexist. A gradual reduction in the α value is usually observed in superconductors as the disorder in the nanoscale increases by adding random point defects [46]. It is important to note that although there is a peak in $J_c(T)$ at high magnetic fields, the α values in the undoped crystals remain at a fairly constant increasing temperature. To understand the origin of the pinning in the undoped sample, it is necessary to consider LT-STM data [29]. The vortex pinning to magnetic fields up 8 T at 0.8 K is produced by defects with a size comparable to ξ. From a geometrical point of view, the crossover from strong to weak pinning occurs when $\sqrt{2}\xi(T) > r_d$ (with r_d the radius of the defect) [32]. Moreover, the pinning can be affected by a reduction in the ξ value when the magnetic field is increased [29].

The $J_c(H)$ dependence at the power law produced by a random distribution of nanoparticles has been theoretically predicted as [47]

$$J_c \approx 0.0866 n_i J_0 \frac{[DF(T)]^{9/4}}{\varepsilon \xi^{1/2}} \left(\frac{\Phi_0}{H}\right)^{5/8}, \quad (1)$$

where n_i is the density of the pinning particles, D is their diameter (assuming that they are spherical), ε the anisotropy parameter, and $F(T) \approx \ln[1 + (D^2/8\xi^2(T))]$. Although for the undoped sample α is slightly larger than 5/8, it is useful to compare the absolute J_c values at low temperatures with the expected density of strong pinning centers. Using $\xi \approx 1.4$ nm and $D = 3–4$ nm, we obtain $F(0) \approx 0.45–0.7$. The $J_c(H)$ average values at 1.8 K (i.e., $1.7\,\mathrm{MA\,cm^{-2}}$ at 0.7 T and $0.43\,\mathrm{MA\,cm^{-2}}$ at 4.5 T) with $J_0 = 170\,\mathrm{MA\,cm^{-2}}$ corresponds to $n_i \approx 1–5 \times 10^{17}\,\mathrm{cm^{-3}}$. These values indicate defects at distances of $\approx$15–20 nm, which is in agreement with LT-STM data where a disordered vortex lattice is observed at magnetic fields up 8 T at 0.8 K (intervortex distance about 18 nm) [29]. A similar analysis may be performed in Ni-doped samples. The differences in the absolute values of J_c are produced by both changes in the superconducting parameters (such as ξ and λ) and variations in the density and size of the crystalline defects.

Regime III should be analyzed considering vortex pinning produced by random disorder [$\sqrt{2}\xi(T) > r_d$] [32]. As we mentioned earlier, the undoped crystal displays modest J_c values at low temperatures and high magnetic fields. Moreover, $J_c(H) \approx$ constant is expected for temperatures below 20 K [23]. The simplest possibility is that regimes I and II are due to a sparse distribution of strong defects, and regime III is due to a denser collection of random point disorder [15]. The disorder caused by Ni substitution at the nanoscale favors the presence of the SPM. The latter is in agreement with the fact that in systems such as $YBa_2Cu_3O_{7-\delta}$ [48] and $Ba(Fe_{1-x}Co_x)_2As_2$ [14], the SPM is suppressed when the local chemical and electronic uniformity increase by thermal annealing. Regime III with $J_c(H) \approx$ constant can be analyzed in terms of the collective pinning by random point disorder as described by the Larkin-Ovchinnikov theory [49].

The theory of weak collective flux pinning predicts several regimes that depend on the vortex-vortex and vortex-defect interactions. In the SVR, the vortex-vortex interaction is negligible compared to the vortex-defect interaction. When the magnetic field is raised, vortex-vortex interactions become dominant, and the vortices are collectively trapped as bundles. The critical current density at the SVR is magnetic field independent and expected to follow

$$J_c \approx J_0 \left(\frac{27 n_d D_v^4}{256 \varepsilon \xi}\right)^{2/3}, \quad (2)$$

where n_d is point defect density, and D_v is the radius of the defects [47]. In the SVR the small-scale displacements of neighboring vortices are independent. The crossover at B^{cr} occurs when the longitudinal displacement correlation length $[L_c^c = \gamma^{-1}\xi(J_0/J_c)^{1/2}]$ is larger than the vortex lattice parameter $[a_0 = 1.07(\Phi_0/B)^{1/2}]$. For the undoped sample, if we used $J_c^{\text{III regime}}(5\,\text{K}) \approx 0.27\,\text{MA cm}^{-2}$, $\xi(0) = 1.4\,\text{nm}$ [26], $\gamma \approx 1$ [50], and $J_0 \approx 170\,\text{MA cm}^{-2}$, we theoretically estimate $B^{cr}(5\,\text{K}) \approx 3.5\,\text{T}$. Although the prediction is qualitatively correct, this value is 1 order of magnitude smaller than the experimental observations with $J_c(H) \approx$ constant at high magnetic fields (>15 T) in Ref. [23]. This fact suggests that other sources of pinning contribute to regime III. Indeed, pinning induced by temperature due to planar $CaFe_2As_2$ inclusions do not modify the α exponent but enhance J_c.

An understanding of the different pinning exhibited by the $CaK(Fe_{1-x}Ni_x)_4As_4$ single crystals is gained from $J_c(T)$ dependences. As we mentioned previously, undoped crystals display a peak at intermediate temperatures in the $J_c(T)$ dependences when $\mu_0 H > 1\,\text{T}$ [see Fig. 3(a)]. This unusual feature is not present in Ni-doped crystals [see Fig. 3(c)]. In addition to the peak at high magnetic fields and temperatures higher than 7 K, the J_c (T/T_c) at $\mu_0 H = 0.3\,\text{T}$ (mostly regime II) for the undoped crystal is smoother than for the doped ones. On the other hand, the curves at $\mu_0 H = 3\,\text{T}$ (mostly regime III) show that although J_c increases with temperature, the absolute values below $T_c/2$ for the undoped crystal are systematically smaller than those observed for x up to 0.03. Thus, the unusual peak in $J_c(T)$ at high fields may be related to a weak pinning scenario in which the temperature induces new pinning centers or an increment in the size of the existent ones [see Eq. (2)]. However, as we mentioned earlier, it has also been associated with pinning provided by $CaFe_2As_2$ inclusions [16]. The effect is not evidenced in Ni-doped samples because the chemical substitution improves the vortex pinning and masks little changes in the pinning landscape. It is important to note that the $J_c(T)$ values in Fig. 3(a) are approximately 4 times smaller than those reported in Ref. [23] for $\approx$2.6-μm-thick $CaKFe_4As_4$ single crystals, indicating that the vortex pinning is affected by the thickness.

To analyze in more detail the J_c (H, T) dependences, we measured the relaxation of persistent currents as a function of time. Fe-SCs usually display a giant flux creep rate that is well described by the collective pinning theory [32]. The pinning energy depends on the pinning potential and the elastic deformation of the vortices. At low temperatures, the vortices are essentially frozen into their distorted configuration. As the temperature increases, the pinning strength decreases as a consequence of the thermal fluctuations of the vortex line. The effective activation energy as a function of current density J is given by

$$U_{\text{eff}} = \frac{U_0}{\mu}\left[\left(\frac{J_c}{J}\right)^{\mu} - 1\right], \tag{3}$$

where U_0 is the collective pinning barrier in the absence of a driving force and μ is the regime-dependent glassy exponent [32]. For elastic creep $\mu > 0$ and for plastic creep $\mu < 0$ [51]. The model of the nucleation of vortex loops predicts for random point defects μ equal to 1/7, 3/2 or 5/2, and

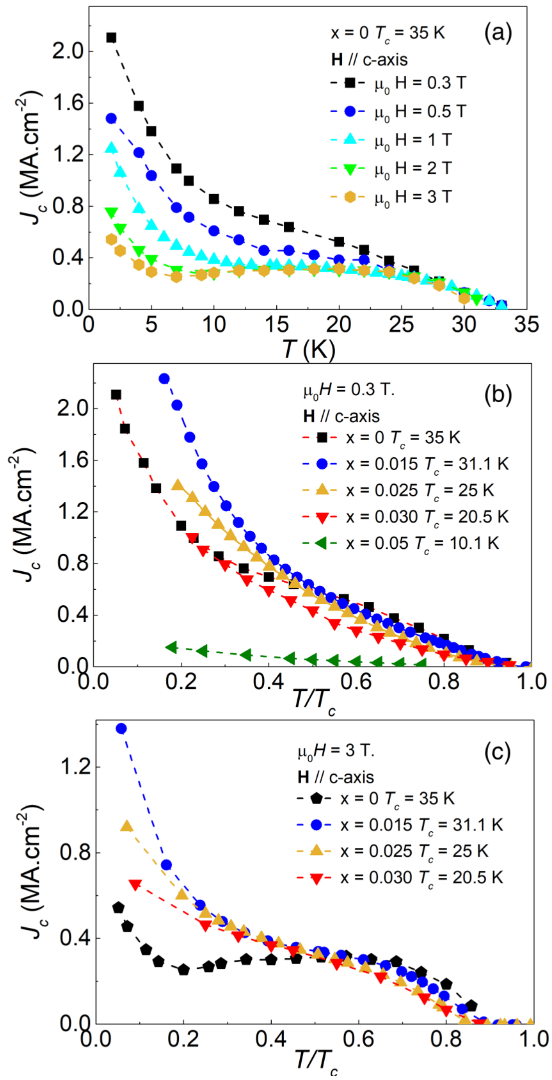

FIG. 3. (a) Temperature dependence of the critical current densities J_c for different applied fields in a $CaKFe_4As_4$ single crystal. (b, c) Reduced temperature dependence of the critical current densities in $CaK(Fe_{1-x}Ni_x)_4As_4$ single crystals at $\mu_0 H = 0.3$ and 3 T, respectively.

7/9 for single-vortex creep, small-bundle creep, or large-bundle creep, respectively [32]. Using Eq. (3), the temperature dependence of the creep rate (S) results in

$$S = -\frac{\delta \ln J}{\delta \ln t} = \frac{T}{U_0 + \mu T \ln\left(\frac{t}{t_0}\right)}, \tag{4}$$

where t is the time and t_0 is an effective hopping attempt time. Equation (4) describes well the presence of a thermally activated Anderson-Kim mechanism at low temperatures ($S \approx T/U_0$) and a plateau in S (T) in the limit of $U_0 \ll \mu T \ln(\frac{t}{t_0})$. Although theoretical models provide a small set of discreet μ values (constant for each regime), experimental studies usually present a gradual evolution of μ from small to large bundles values as H is increased [52]. The glassy exponents μ can be obtained from S (T) data using the extended Maley method [33]. Approximating the current density decays as $\frac{dJ}{dt} = -(\frac{J_c}{\tau})e^{-\frac{U_{\text{eff}}(J)}{T}}$, the effective activation energy $U_{\text{eff}}(J)$ can

TABLE II. Summary of the glassy exponent μ (left), U_0 (middle), and J_c (right) obtained from Maley analysis. The error bar is of 0.03. (*) and (#) indicate regimes II and III, respectively. The error bars in U_0 are ≈10%.

	0.015			0.025			0.03			0.05		
$CaK(Fe_{1-x}Ni_x)_4As_4$	μ	U_0	J_c	μ	U_0	J_c	μ	U_0	J_c	μ	U_0	J_c
0.1 T										0.54*	60	0.42
0.3 T	0.55*	90	5.0	0.62*	110	3.3	0.69*	95	2.2	0.97#	38	0.33
1 T	0.64*	55	4.2	1.04*	70	2.2	1.25*	45	1.8			

be experimentally obtained by $U_{\mathrm{eff}} = -T[\ln|\frac{dJ}{dt}| - C]$ (with $C = \ln(J_c/\tau)$ a constant factor). To maintain "piecewise" continuity at high T, U_{eff} is divided by a thermal factor $G(T) \leqslant 1$ [53]. In the following the flux creep data and analysis of the glassy exponents will be presented. The summary of μ and U_0 is presented in Table II.

Figure 4(a) shows $S(T)$ in a $CaKFe_4As_4$ single crystal at $\mu_0 H = 0.3$, 0.5, 1, and 3 T (top x axis shows the data in T/T_c). Typical curves of $J(T)$ are shown in Appendix. The qualitative features of the $S(T)$ curves are similar to previous observations in Fe-SCs and YBCO single crystals [12–14,54]. The main characteristics are the large S values (low U_0 values) and modulations in $S(T)$ (crossovers between vortex regimes). The initial increase of $S(T)$ corresponds to an Anderson-Kim–like creep with $S \approx T/U_0$, except that the nonzero extrapolation to $S(T=0)$ is usually attributed to a

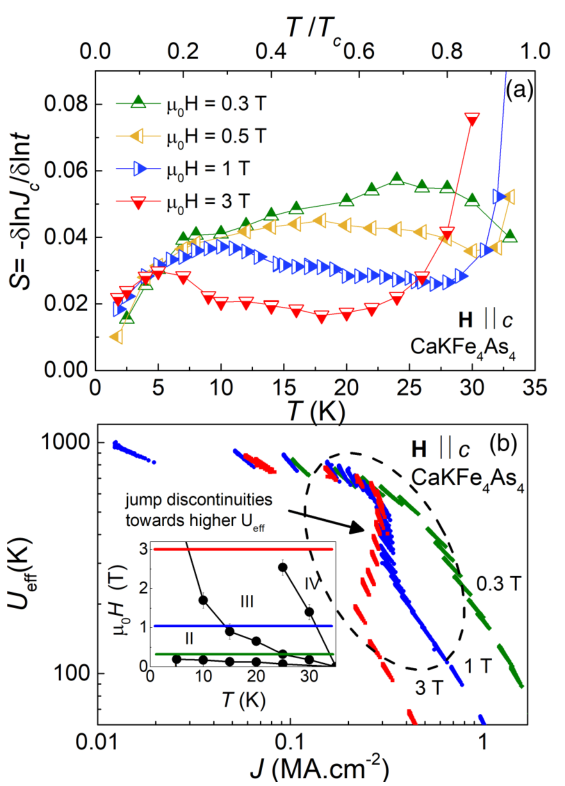

FIG. 4. (a) Creep rate (S) vs temperature (bottom x axis) and reduced temperature T/T_c (top x axis) at different applied magnetic fields for a $CaKFe_4As_4$ single crystal. (b) Maley analysis with $\mu_0 H = 0.3$, 1, and 3 T. The data is obtained with $G(T) = 1$. Inset shows an H-T phase diagram with the $J_c(H)$ regimes indicated in Fig. 2(b). The data is obtained using $C = 13$.

quantum creep component. The quantum creep contribution may be estimated by $S^Q \cong \frac{e^2}{\hbar}\frac{\rho_n}{\xi}(\frac{J_c}{J_0})^{1/2}$, where ρ_n is the resistance in the normal state, J_0 is the depairing critical current density, and $\frac{\hbar}{e^2} = 4108\,\Omega$ [32]. Using $\rho_n = 20\,\mu\,\Omega\,\mathrm{cm}$ [26], $J_0 = 170\,\mathrm{MA\,cm^{-2}}$, $J_c(0.3\,\mathrm{T}) \approx 2\,\mathrm{MA\,cm^{-2}}$, and $J_c(3\,\mathrm{T}) \approx 0.5\,\mathrm{MA\,cm^{-2}}$, the S^Q values should be in the range of 0.004–0.002. At intermediate temperatures the flux creep rates depend on the applied magnetic fields. The $S \sim 0.017–0.067$ values are characteristic of collective creep of vortex bundles. The gradual reduction in the S values as the field increases suggests an increment in the glassy exponent μ [52,54]. At temperatures near T_c, the flux creep rates start to be faster as a consequence of change from elastic to plastic relaxation [12]. Figure 4(b) shows the Maley analysis [with $G(T) = 1$] for $\mu_0 H = 0.3$, 1, and 3 T. The results show unusual behavior in which $U_{\mathrm{eff}}(J)$ displays jumplike discontinuities towards higher U_{eff} values as J decreases. The effect appears both for magnetic fields within regimes II and III [see inset Fig. 4(b)]. To explain the observed variations it is necessary to consider that U_0 and J_c increase as the temperature rises [see Eq. (3)], indicating the appearance of new pinning centers or a change in the size of the existing ones. This fact is in agreement with the peak in $J_c(T)$ for high magnetic fields discussed above. The U_0 value can be estimated for weak pinning in the SVR by $U_c \approx \frac{H_c^2\xi^3}{\gamma}(\frac{J_c}{J_0})^{1/2}$. An estimate for 10 K in regime III using $\xi(0) = 1.4\,\mathrm{nm}$ [26], $\gamma \approx 1.2$, $\lambda \approx 200$ nm [28], and $J_c(10\,\mathrm{K}) \approx 0.3\,\mathrm{MA\,cm^{-2}}$ yields $U_0 \approx 50\,\mathrm{K}$. As we mentioned earlier, low U_0 values are consistent with the large S values observed even for low temperatures [i.e., $S(5\,\mathrm{K}) \approx 0.03$].

The flux creep relaxation rates S and the Maley analysis for Ni-doped samples are shown in Figs. 5 ($x = 0.015$), 6 ($x = 0.025$), 7 ($x = 0.03$), and 8 ($x = 0.05$). Panels (a) correspond to $S(T)$ measurements at $\mu_0 H = 0.3$, 1, and 3 T (top x axis shows the data in T/T_c). For $x = 0.05$, due to the shorter extension of the different regimes, the measurements were performed at $\mu_0 H = 0.1$, 0.3, and 0.5 T. Panels (b) and (c) display the conventional and extended Maley analysis, respectively. Inset panels (b) and (c) show the H-T phase diagram indicating the crossovers between vortex regimes and the $G(T)$ function used to maintain "piecewise" continuity, respectively.

The $S(T)$ dependences displayed in the (a) panels of Figs. 5–8 show features similar to those found for the undoped crystal. The curves usually display a peak at the temperature where there is a crossover from regimes II to III. Moreover, the curves at different fields shift to smaller S values. For example, $S(T_c/2)$ at 3 T is 0.026 for $x = 0.015$, 0.022 for $x = 0.025$, and 0.018 for $x = 0.03$. The changes in the S

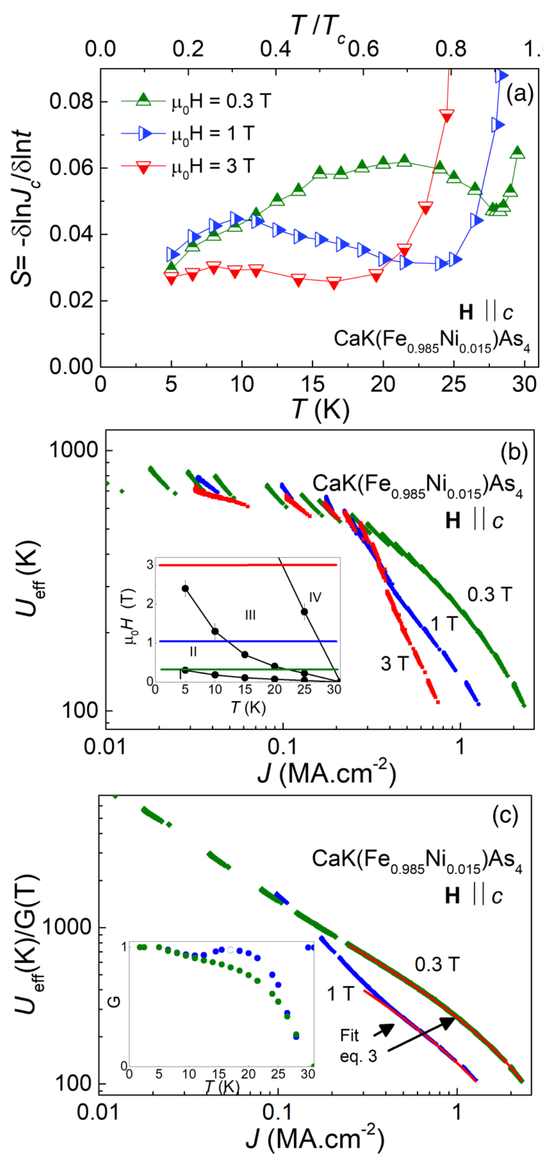

FIG. 5. (a) Creep rate (S) vs temperature (bottom x axis) and reduced temperature T/T_c (top x axis) at different applied magnetic fields for a $CaK(Fe_{0.985}Ni_{0.015})_4As_4$ single crystal. (b) Maley analysis with $\mu_0H = 0.3$, 1, and 3 T. The data is obtained with $G(T) = 1$. Inset shows an H-T phase diagram with the $J_c(H)$ regimes indicated in Fig. 2(b). (c) Extended Maley for $\mu_0H = 0.3$ and 1 T from curves displayed in panel (b). Fits using Eq. (3) are indicated. Inset shows the $G(T)$ function used to normalize U_0. The data is obtained using $C = 13$.

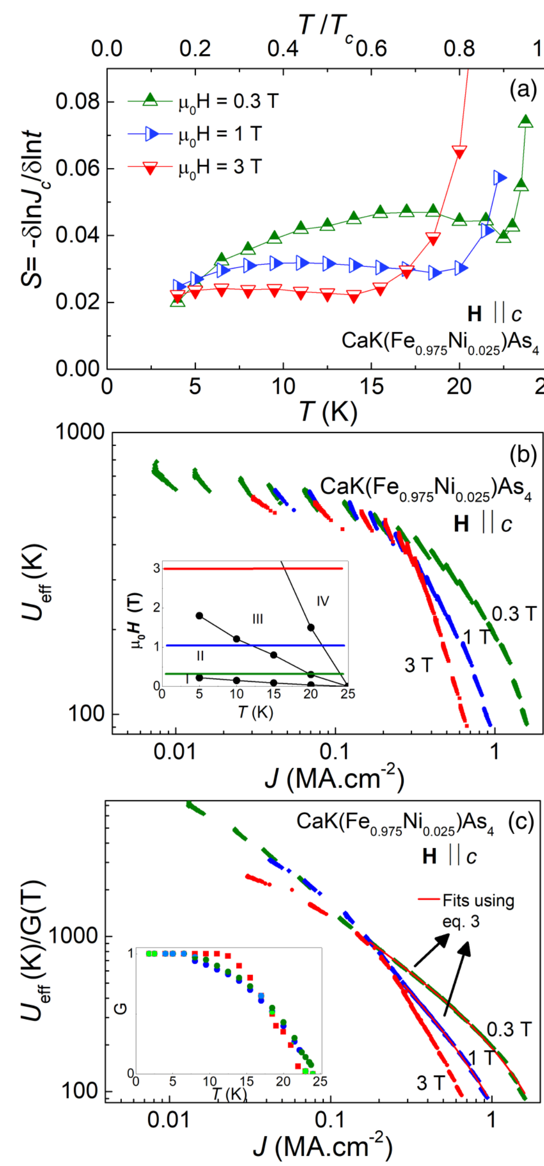

FIG. 6. (a) Creep rate (S) vs temperature (bottom x axis) and reduced temperature T/T_c (top x axis) at different applied magnetic fields for a $CaK(Fe_{0.975}Ni_{0.025})_4As_4$ single crystal. (b) Maley analysis with $\mu_0H = 0.3$, 1, and 3 T. The data is obtained with $G(T) = 1$. Inset shows an H-T phase diagram with the $J_c(H)$ regimes indicated in Fig. 2(c). (c) Extended Maley for $\mu_0H = 0.3$ and 1 T from curves displayed in panel (b). Fits using Eq. (3) are indicated. Inset shows the $G(T)$ function used to normalize U_0. The data is obtained using $C = 13$.

values with temperature and fields may be related to changes in the glassy exponent μ. In systems such as $YBa_2Cu_3O_7$ its value evolves from ≈1/7 (theoretical prediction for SVR) to ≈3/2 at the SPM maximum (theoretical prediction for small bundles) [52,54].

The extended Maley analysis of data displayed in the (b) panels of Figs. 5–8 is shown in panels (c). Like the undoped crystal, U_0 in regime III changes with temperature. For instance, U (J) for $x = 0.015$ at $\mu_0H = 3$ T shows jump discontinuities towards higher $U_{\rm eff}$ as J decreases [see Fig. 5(b)]. Moreover, for 1 T at $T > 12$ K (regime III) the piecewise continuity is maintained with an unusual G (T) [see inset Fig. 5(c)]. Furthermore, the G (T) dependences used to maintain piecewise continuity at $\mu_0H = 3$ T in $x = 0.025$ and 0.03 are different to those used at smaller fields. We analyze the glassy exponent μ and U_0 at regime II using Eq. (3). For $x = 0.015$, 0.025, and 0.03 the analysis was performed at $\mu_0H = 0.3$ and 1 T, and for $x = 0.05$ at $\mu_0H = 0.1$ and 0.3 T. The results are summarized in Table II. The fits are indicated in the (c) panels of Figs. 5–8. The μ value for 0.3 T evolves from 0.55 to 0.97 when x increases from 0.015 to 0.05. Moreover for 1 T, it increases from 0.64 to 1.25 when

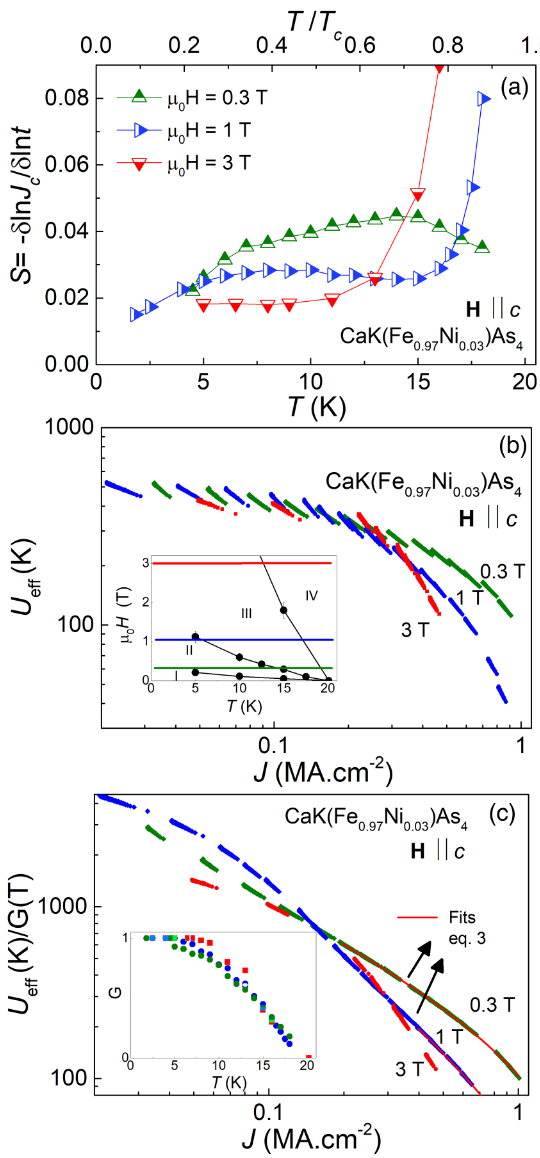

FIG. 7. (a) Creep rate (S) vs temperature (bottom x axis) and reduced temperature T/T_c (top x axis) at different applied magnetic fields for a $CaK(Fe_{0.97}Ni_{0.03})_4As_4$ single crystal. (b) Maley analysis with $\mu_0H = 0.3$, 1, and 3 T. The data is obtained with $G(T) = 1$. Inset shows an H-T phase diagram with the $J_c(H)$ regimes indicated in Fig. 2(c). (c) Extended Maley for $\mu_0H = 0.3$ and 1 T from curves displayed in panel (b). Fits using Eq. (3) are indicated. Inset shows the $G(T)$ function used to normalize U_0. The data is obtained using $C = 13$.

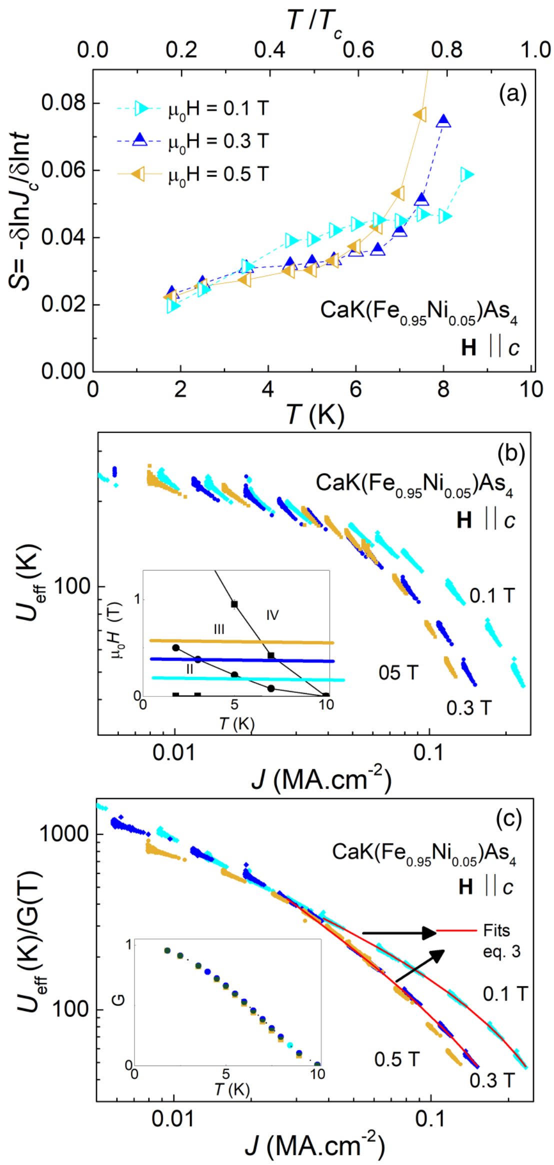

FIG. 8. (a) Creep rate (S) vs temperature (bottom x axis) and reduced temperature T/T_c (top x axis) at different applied magnetic fields for a $CaK(Fe_{0.95}Ni_{0.05})_4As_4$ single crystal. (b) Maley analysis with $\mu_0H = 0.1, 0.3$, and 0.5 T. The data is obtained with $G(T) = 1$. Inset shows an H-T phase diagram with the $J_c(H)$ regimes indicated in Fig. 2(e). (c) Extended Maley for the curves displayed in panel (b). Fits using Eq. (3) are indicated. Inset shows the G (T) function used to normalize U_0. The data is obtained using $C = 13$.

x increases from 0.015 to 0.03. The evolution of μ (x) at the same field may be related to different scales in H/H_{c2} and a gradual crossover from values predicted for SVR (1/7) and small bundles (3/2) [52,54], indicating similar pinning mechanisms over the whole range of compositions. There are no particular features that can be related to the coexistence of superconductivity and AFM. The influence of T_c and related parameters such as H_{c2} in the μ (x) dependence is clearly evident for $\mu^{0.3\,T} = 0.55(0.03)$ in $x = 0.015$ (with $T_c = 31$ K) and $\mu^{0.1\,T} = 0.54$ (0.03) in $x = 0.05$ (with $T_c = 10.1$ K). The low U_0 values (typically <100 K) contribute to the large S values displayed for all the samples over the whole range of temperature. Moreover, we observed that U_0 decreases as the field increases, indicating that the changes in the absolute S values with magnetic fields at low temperatures are mainly related to changes in μ [see Eq. (4)]. For the undoped crystals, due to the similarity in the S (T) dependences, the glassy exponents μ and U_0 are expected to be of the same order than in Ni-doped samples. The main differences may be related to both the small coherence length ξ and the absence of extended pinning centers. Slight modifications in the pinning landscape of the undoped crystals improve the pinning, as is evidenced in the peak at the $J_c(T)$ dependences. Small Ni addition

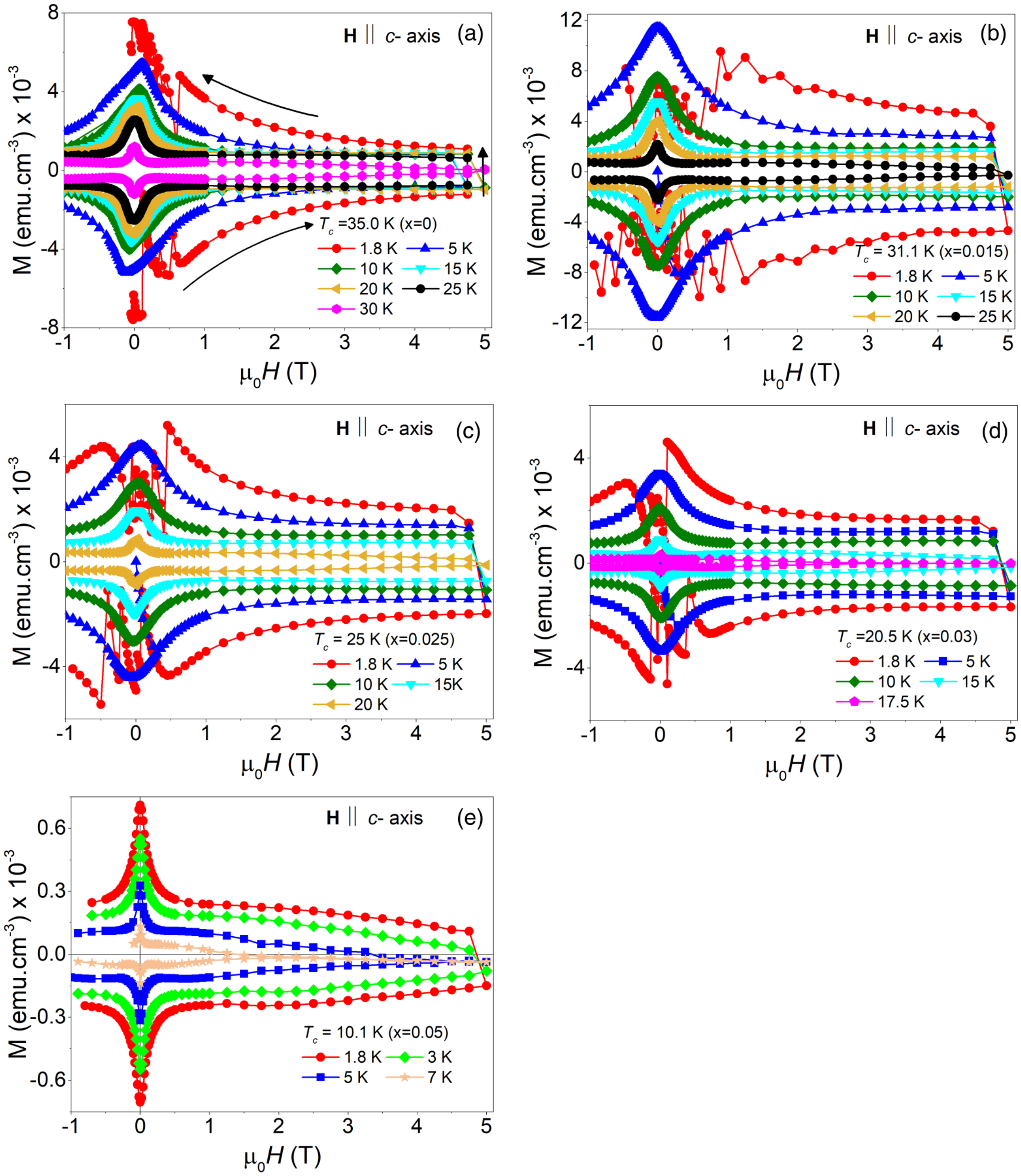

FIG. 9. (a)–(e) Magnetization loops with $\mathbf{H}\|c$ in Ni-doped $CaK(Fe_{1-x}Ni_x)_4As_4$ ($x = 0$, 0.015, 0.025, 0.03, and 0.05) single crystals at several temperatures. The curves correspond to magnetic fields between $\mu_0 H = -1$ and 5 T.

increases the disorder, masking small variations in the pinning landscape with temperature. Nevertheless, the Maley analysis indicates that U_0 at regime III also changes for the doped samples. Considering that planar $CaFe_2As_2$ intergrowths are over the entire range of chemical compositions [16], their contribution to the vortex pinning is stronger for undoped crystals.

Finally, it is important to mention that, as is evidenced from Figs. 2(a) and 2(b), the J_c values in the undoped crystals may be significantly enhanced by adding pinning centers. One of the most effective methods to improve pinning in superconductors with short ξ is particle irradiation [4]. Depending on the mass and energy of the ions and for an adequate dose, U_0 in Fe-SCs may increase from tens of Kelvins to 300–500 K [4,14]. The value $J_c^{sf}(5\,\mathrm{K}) \approx 1.7 - 2\,\mathrm{MA\,cm^{-2}}$ in $CaKFe_4As_4$ is similar that found in single crystals of $YBa_2Cu_3O_{7-d}$ ($\approx 2\,\mathrm{MA\,cm^{-2}}$ [55]) and $Ba_{0.6}K_{0.4}Fe_2As_2$ ($\approx 2\,\mathrm{MA\,cm^{-2}}$ [56]). Moreover, the value duplicates the typically observed in optimal doped $Ba(Fe,Co)_2As_2$ [14]. As was previously noticed, $CaKFe_4As_4$ single crystals display high anisotropy in the pinning properties due to planar defects [16,17,23]. The presence of $CaFe_2As_2$ intergrowths considerably improves J_c for $\mathbf{H}//ab$ [16,17]. Furthermore, comparison with previously reported data in thinner single crystals suggests that the pinning mechanisms are strongly affected by thickness [23].

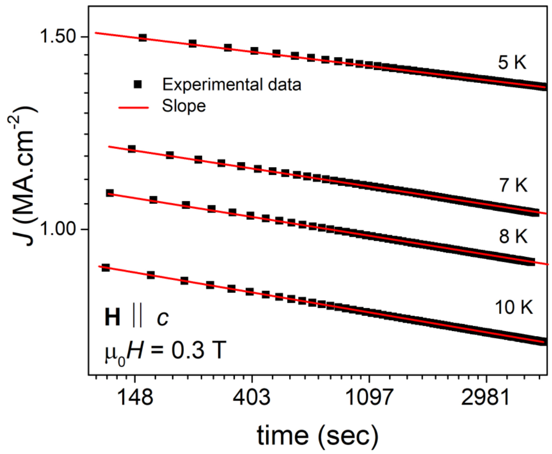

FIG. 10. Current density J as a function of time (logarithmic scales) for $T = 5$, 7, 8, and 10 K for a $CaKFe_4As_4$ single crystal with $\mu_0 H = 0.3$ T applied $\mathbf{H}||c$.

IV. CONCLUSION

We have performed magnetic measurements on single crystals of $CaK(Fe_{1-x}Ni_x)_4As_4$ ($x \approx 0$, 0.015, 0.025, 0.03, and 0.05). The $J_c(H)$ dependences usually display a power-law regime followed by a SPM. The magnetic relaxation of all the crystals is well described by the collective creep theory. The samples display the glassy exponent μ within predictions for vortex bundles in a weak pinning scenario and relatively small characteristic pinning energy ($U_0 < 100$ K). Comparatively, the undoped crystals display low J_c values at high magnetic fields and low temperatures. Small Ni doping improves the vortex pinning and enhances J_c in the whole range of magnetic fields. The self-field J_c shows a discontinuous break to smaller values as the samples develop an AFM ordered ground state that coexists with a competing superconducting state. Moreover, the magnetic field dependences of J_c at intermediate values are more gradual as Ni doping increases. These changes are smoother for $x > 0.015$, suggesting that AFM domains affect the vortex pinning. The undoped crystal displays an unusual peak in $J_c(T)$ at high fields. The enhancement in $J_c(T)$ matches with an unexpected increase in U_0 and the appearance of a SPM. Ni doping induces a SPM in the $J_c(H)$ dependences for the whole range of temperature. The analysis of the vortex dynamics for small and intermediate magnetic fields shows a gradual evolution in the glassy exponent μ with Ni content x. This implies that there is no appreciable change in the mechanism that determines the vortex relaxation for Ni-doped samples with and without magnetic order. The large J_c values observed in the undoped crystal, even for low chemical disorder, suggest that they can be significantly enhanced by adding pinning centers.

ACKNOWLEDGMENTS

This work was supported by the US Department of Energy, Office of Basic Energy Science, Division of Materials Sciences and Engineering. The research was performed at the Ames Laboratory. Ames Laboratory is operated for the U.S. Department of Energy by Iowa State University under Contract No. DE-AC02-07CH11358. W.R.M. was supported by the Gordon and Betty Moore Foundation's EPiQS Initiative through Grant No. GBMF4411. N.H. is partially supported by ANCYP PICT2015-2171 (Argentina).

APPENDIX

The critical current densities J_c were estimated from the Bean model using the appropriate geometrical factor in the Bean model [35,36]. Figure 9 shows the hysteresis loops under $\mathbf{H}||c$ in Ni-doped $CaK(Fe_{1-x}Ni_x)_4As_4$ single crystals at several temperatures. The curves are obtained for magnetic fields between μ_0H = −1 T and $\mu_0 H = 5$ T. For each temperature before starting the measurements, an initial negative magnetic field $H \sim 4H^p$ is applied (to guarantee the critical state at the first point).

The flux creep rates were obtained as $S = -(\delta \ln J/\delta \ln t)$ from the time dependence of the magnetization at different fields and temperatures. Figure 10 shows typical curves of J (time) for a $CaKFe_4As_4$ single crystal.

[1] R. Willa, A. E. Koshelev, I. A. Sadovskyy, and A. Glatz, Phys. Rev. B **98**, 054517 (2018).

[2] H. Hosono, A. Yamamoto, H. Hiramatsu, and Y. Ma, Mater. Today **21**, 278 (2018).

[3] L. Fang, Y. Jia, J. A. Schlueter, A. Kayani, Z. L. Xiao, H. Claus, U. Welp, A. E. Koshelev, G. W. Crabtree, and W.-K. Kwok, Phys. Rev B **84**, 140504(R) (2011).

[4] W.-K. Kwok, U. Welp, A. Glatz, A. E. Koshelev, K. J. Kihlstrom, and G. W. Crabtree, Rep. Prog. Phys. **79**, 116501 (2016).

[5] I. I. Mazin, Nature (London) **464**, 183 (2010).

[6] X. Chen, P. Dai, D. Feng, T. Xiang, and F.-C. Zhang, Natl. Sci. Rev. **1**, 371 (2014).

[7] K. Kudo, K. Iba, M. Takasuga, Y. Kitahama, J.-i. Matsumura, M. Danura, Y. Nogami, and M. Nohara, Sci. Rep. **3**, 1478 (2013).

[8] A. Chubukov and P. J. Hirschfeld, Phys. Today **68**(6), 46 (2015).

[9] H. Okabe, N. Takeshita, K. Horigane, T. Muranaka, and J. Akimitsu, Phys. Rev. B **81**, 205119 (2010).

[10] S. K. Kim, M. S. Torikachvili, E. Colombier, A. Thaler, S. L. Bud'ko, and P. C. Canfield, Phys. Rev B **84**, 134525 (2011).

[11] S. L. Bud'ko, Y. Liu, T. A. Lograsso, and P. C. Canfield, Phys. Rev. B **86**, 224514 (2012).

[12] R. Prozorov, N. Ni, M. A. Tanatar, V. G. Kogan, R. T. Gordon, C. Martin, E. C. Blomberg, P. Prommapan, J. Q. Yan, S. L. Bud'ko, and P. C. Canfield, Phys. Rev. B **78**, 224506 (2008).

[13] Y. Nakajima, Y. Tsuchiya, T. Taen, T. Tamegai, S. Okayasu, and M. Sasase, Phys. Rev. B **80**, 012510 (2009).

[14] N. Haberkorn, J. Kim, K. Gofryk, F. Ronning, A. S. Sefat, L. Fang, U. Welp, W. K. Kwok, and L. Civale, Supercond. Sci. Technol. **28**, 055011 (2015).

[15] C. J. van der Beek, G. Rizza, M. Konczykowski, P. Fertey, I. Monnet, T. Klein, R. Okazaki, M. Ishikado, H. Kito, A. Iyo, H. Eisaki, S. Shamoto, M. E. Tillman, S. L. Bud'ko, P. C. Canfield, T. Shibauchi, and Y. Matsuda, Phys. Rev B **81**, 174517 (2010).
[16] S. Ishida, A. Iyo, H. Ogino, H. Eisaki, N. Takeshita, K. Kawashima, K. Yanagisawa, Y. Kobayashi, K. Kimoto, H. Abe, M. Imai, J.-i. Shimoyama, and M. Eisterer, npj Quantum Mater. **4**, 27 (2019).
[17] S. Pyon, A. Takahashi, I. Veshchunov, T. Tamegai, S. Ishida, A. Iyo, H. Eisaki, M. Imai, H. Abe, T. Terashima, and A. Ichinose, Phys. Rev B **99**, 104506 (2019).
[18] C.-L. Song, Y.-L. Wang, Y.-P. Jiang, L. Wang, K. He, X. Chen, J. E. Hoffman, X.-C. Ma, and Q.-K. Xue, Phys. Rev. Lett. **109**, 137004 (2012).
[19] W.-H. Jiao, Q. Tao, Z. Ren, Y. Liu, and G.-H. Cao, npj Quantum Mater. **2**, 50 (2017).
[20] V. S. Stolyarov, I. S. Veshchunov, S. Yu. Grebenchuk, D. S. Baranov, I. A. Golovchanskiy, A. G. Shishkin, N. Zhou, Z. Shi, X. Xu, S. Pyon, Y. Sun, W. Jiao, G.-H. Cao, L. Ya. Vinnikov, A. A. Golubov, T. Tamegai, A. I. Buzdin, and D. Roditchev, Sci. Adv. **4**, 1061 (2018).
[21] S. L. Bud'ko, V. G. Kogan, R. Prozorov, W. R. Meier, M. Xu, and P. C. Canfield, Phys. Rev B **98**, 144520 (2018).
[22] W. Cheng, H. Lin, B. Shen, and H.-H. Wen, Sci. Bull. **64**, 81 (2019).
[23] S. J. Singh, M. Bristow, W. R. Meier, P. Taylor, S. J. Blundell, P. C. Canfield, and A. I. Coldea, Phys. Rev. Mater. **2**, 074802 (2018).
[24] A. Iyo, K. Kawashima, T. Kinjo, T. Nishio, S. Ishida, H. Fujihisa, Y. Gotoh, K. Kihou, H. Eisaki, and Y. Yoshida, J. Am. Chem. Soc. **138**, 3410 (2016).
[25] D. Mou, T. Kong, W. R. Meier, F. Lochner, L.-L. Wang, Q. Lin, Y. Wu, S. L. Bud'ko, I. Eremin, D. D. Johnson, P. C. Canfield, and A. Kaminski, Phys. Rev. Lett. **117**, 277001 (2016).
[26] W. R. Meier, T. Kong, U. S. Kaluarachchi, V. Taufour, N. H. Jo, G. Drachuck, A. E. Bohmer, S. M. Saunders, A. Sapkota, A. Kreyssig, M. A. Tanatar, R. Prozorov, A. I. Goldman, F. F. Balakirev, A. Gurevich, S. L. Bud'ko, and P. C. Canfield, Phys. Rev. B **94**, 064501 (2016).
[27] U. S. Kaluarachchi, V. Taufour, A. Sapkota, V. Borisov, T. Kong, W. R. Meier, K. Kothapalli, B. G. Ueland, A. Kreyssig, R. Valentí, R. J. McQueeney, A. I. Goldman, S. L. Bud'ko, and P. C. Canfield, Phys. Rev. B **96**, 140501(R) (2017).
[28] R. Khasanov, W. R. Meier, Y. Wu, D. Mou, S. L. Bud'ko, I. Eremin, H. Luetkens, A. Kaminski, P. C. Canfield, and A. Amato, Phys. Rev. B **97**, 140503(R) (2018).
[29] A. Fente, W. R. Meier, T. Kong, V. G. Kogan, S. L. Bud'ko, P. C. Canfield, I. Guillamón, and H. Suderow, Phys. Rev. B **97**, 134501 (2018).
[30] W. R. Meier, Q.-P. Ding, A. Kreyssig, S. L. Bud'ko, A. Sapkota, K. Kothapalli, V. Borisov, R. Valentí, C. D. Batista, P. P. Orth, R. M. Fernandes, A. I. Goldman, Y. Furukawa, A. E. Böhmer, and P. C. Canfield, npj Quantum Mater. **3**, 5 (2018).
[31] A. Kreyssig, J. M. Wilde, A. E. Böhmer, W. Tian, W. R. Meier, Bing Li, B. G. Ueland, Mingyu Xu, S. L. Bud'ko, P. C. Canfield, R. J. McQueeney, and A. I. Goldman, Phys. Rev. B **97**, 224521 (2018).
[32] G. Blatter, M. V. Feigel'man, V. B. Geshkenbein, A. I. Larkin, and V. M. Vinokur, Rev. Mod. Phys. **66**, 1125 (1994).
[33] M. P. Maley, J. O. Willis, H. Lessure, and M. E. McHenry, Phys. Rev. B **42**, 2639 (1990).
[34] W. R. Meier, T. Kong, T. S. L. Bud'ko, and P. C. Canfield, Phys. Rev. Mater. **1**, 013401 (2017).
[35] C. P. Bean, Phys. Rev. Lett. **8**, 250 (1962); Rev. Mod. Phys. **36**, 31 (1964).
[36] E. M. Gyorgy, R. B. Van Dover, K. A. Jackson, L. F. Schneemeyer, and J. V. Waszczak, Appl. Phys. Lett. **55**, 283 (1989).
[37] Y. Yeshurun, A. P. Malozemoff, and A. Shaulov, Rev. Mod. Phys. **68**, 911 (1996).
[38] F. Ohtake, T. Taen, S. Pyon, T. Tamegai, S. Okayasu, T. Kambara, and H. Kitamura, Physica C **518**, 47 (2015).
[39] N. Haberkorn, B. Maiorov, I. O. Usov, M. Weigand, W. Hirata, S. Miyasaka, S. Tajima, N. Chikumoto, K. Tanabe, and Leonardo Civale, Phys. Rev. B **85**, 014522 (2012).
[40] R. Prozorov, M. A. Tanatar, N. Ni, A. Kreyssig, S. Nandi, S. L. Bud'ko, A. I. Goldman, and P. C. Canfield, Phys. Rev. B **80**, 174517 (2009).
[41] B. Shen, P. Cheng, Z. Wang, L. Fang, C. Ren, L. Shan, and H.-H. Wen, Phys. Rev. B **81**, 014503 (2010).
[42] D. Song, S. Ishida, A. Iyo, M. Nakajima, J.-i. Shimoyama, M. Eisterer, and H. Eisaki, Sci. Rep. **6**, 26671 (2016).
[43] S. Salem-Sugui, Jr., L. Ghivelder, A. D. Alvarenga, L. F. Cohen, K. A. Yates, K. Morrison, J. L. Pimentel, Jr., H. Luo, Z. Wang, and H.-H. Wen, Phys. Rev. B **82**, 054513 (2010).
[44] F. Hengstbergera, M. Eisterer, and H. W. Weber, Appl. Phys. Lett. **96**, 022508 (2010).
[45] N. Haberkorn, M. Miura, B. Maiorov, G. F. Chen, W. Yu, and L. Civale, Phys. Rev. B **84**, 094522 (2011).
[46] N. Haberkorn, J. Kim, S. Suárez, J.-H. Lee, and S. H. Moon, Supercond. Sci. Technol. **28**, 125007 (2015).
[47] C. J. van der Beek, M. Konczykowski, A. Abal'oshev, I. Abal'osheva, P. Gierlowski, S. J. Lewandowski, M. V. Indenbom, and S. Barbanera, Phys. Rev. B **66**, 024523 (2002).
[48] A. Oka, S. Koyama, T. Izumi, Y. Shiohara, J. Shibata, and T. Hirayama, Jpn. J. Appl. Phys. **39**, 5822 (2000).
[49] A. I. Larkin and Yu. N. Ovchinnikov, J. Low Temp. Phys. **34**, 409 (1979).
[50] H. Q. Yuan, J. Singleton, F. F. Balakirev, S. A. Baily, G. F. Chen, J. L. Luo, and N. L. Wang, Nature (London) **457**, 565 (2009).
[51] Y. Abulafia, A. Shaulov, Y. Wolfus, R. Prozorov, L. Burlachkov, Y. Yeshurun, D. Majer, E. Zeldov, H. Wühl, V. B. Geshkenbein, and V. M. Vinokur, Phys. Rev. Lett. **77**, 1596 (1996).
[52] J. R. Thompson, Y. R. Sun, D. K. Christen, L. Civale, A. D. Marwick, and F. Holtzberg, Phys. Rev. B **49**, 13287(R) (1994).
[53] J. G. Ossandon, J. R. Thompson, D. K. Christen, B. C. Sales, Yangren Sun, and K. W. Lay, Phys. Rev. B **46**, 3050 (1992).
[54] L. Civale, L. Krusin-Elbaum, J. R. Thompson, and F. Holtzberg, Phys. Rev. B **50**, 7188 (1994).
[55] L. Civale, A. D. Marwick, T. K. Worthington, M. A. Kirk, J. R. Thompson, L. Krusin-Elbaum, Y. Sun, J. R. Clem, and F. Holtzberg, Phys. Rev. Lett. **67**, 648 (1991).
[56] L. Fang, Y. Jia, C. Chaparro, G. Sheet, H. Claus, M. A. Kirk, A. E. Koshelev, U. Welp, G. W. Crabtree, W. K. Kwok, S. Zhu, H. F. Hu, J. M. Zuo, H.-H. Wen, and B. Shen, Appl. Phys. Lett. **101**, 012601 (2012).